AIP | The Journal of Chemical Physics

KAg11(VO4)4 as a candidate p-type transparent conducting oxide

Jino Im, Giancarlo Trimarchi, Haowei Peng, Arthur J. Freeman, Veerle Cloet et al.

Citation: J. Chem. Phys. **138**, 194703 (2013); doi: 10.1063/1.4804556
View online: http://dx.doi.org/10.1063/1.4804556
View Table of Contents: http://jcp.aip.org/resource/1/JCPSA6/v138/i19
Published by the AIP Publishing LLC.

Additional information on J. Chem. Phys.

Journal Homepage: http://jcp.aip.org/
Journal Information: http://jcp.aip.org/about/about_the_journal
Top downloads: http://jcp.aip.org/features/most_downloaded
Information for Authors: http://jcp.aip.org/authors

ADVERTISEMENT

Downloaded 24 Jun 2013 to 192.174.37.50. This article is copyrighted as indicated in the abstract. Reuse of AIP content is subject to the terms at: http://jcp.aip.org/about/rights_and_permissions

$KAg_{11}(VO_4)_4$ as a candidate *p*-type transparent conducting oxide

Jino Im,[1,a)] Giancarlo Trimarchi,[1] Haowei Peng,[1] Arthur J. Freeman,[1] Veerle Cloet,[2] Adam Raw,[2] and Kenneth R. Poeppelmeier[2]
[1]*Department of Physics and Astronomy, Northwestern University, Evanston, Illinois 60208, USA*
[2]*Department of Chemistry, Northwestern University, Evanston, Illinois 60208, USA*

(Received 25 January 2013; accepted 26 April 2013; published online 16 May 2013)

For a material to be a good *p*-type transparent conducting oxide (TCO), it must *simultaneously* satisfy several design principles regarding its bulk and defect phase thermochemistry, its optical absorption spectrum, and its electric transport properties. Recently, we predicted Ag_3VO_4 to be *p*-type but with low conductivity and an optical band gap not large enough for transparency. To improve on the transport and optical properties of Ag_3VO_4, we searched an extended material space including quaternary compounds based on Ag, V, O, and an additional atom for a new candidate *p*-type TCO. From this set of quaternary materials, we selected $KAg_{11}(VO_4)_4$, a known oxide with a crystal structure related to that of Ag_3VO_4. Notably, one could expect a possible enhancement of the concentration of hole producing Ag-vacancy defects in $KAg_{11}(VO_4)_4$ due to its different local geometries of Ag atoms (2- and 3-fold coordinated) with respect to the 4-fold coordinated Ag atoms in Ag_3VO_4. By performing first-principles calculations, we found that $KAg_{11}(VO_4)_4$ is an intrinsic *p*-type conductor and can be synthesized under conditions similar to those predicted for the synthesis of Ag_3VO_4. However, we predict that the intrinsic hole content in $KAg_{11}(VO_4)_4$ is similar to that in Ag_3VO_4 even though $KAg_{11}(VO_4)_4$ contains 2- and 3-fold coordinated Ag, hole producing sites with a lower defect formation energy than the 4-fold coordinated one. Our calculation demonstrates that the advantage from lower coordination number of the Ag atom in $KAg_{11}(VO_4)_4$ can be offset by the change in the range of Ag chemical potential in which synthesis is allowed due to the oxide phases that Ag forms with K and that energetically compete with $KAg_{11}(VO_4)_4$. © *2013 AIP Publishing LLC*. [http://dx.doi.org/10.1063/1.4804556]

I. THE SEARCH FOR *p*-TYPE TRANSPARENT CONDUCTIVE OXIDES DRIVEN BY DESIGN PRINCIPLES

Materials that are electron (*n*-type) or hole (*p*-type) conductors *and* transparent to visible light, so called transparent conducting oxides (TCOs), are enabling the development of transparent electronics[1] and are also crucial in photovoltaic technologies.[2] *p*-type TCOs are essential along with the *n*-type ones to design transparent electronic devices, however, in contrast to the *n*-type TCOs, very few *p*-type TCOs have so far been discovered. This has generated much interest in the solid-state chemistry and materials science communities to search for new *p*-type TCOs with improved optical and transport properties. Ideally such compounds should include elements that are plentiful (earth-abundant) and non-toxic (earth-friendly).

The discovery of an intrinsic hole conductivity of 1 S/cm in thin films of the transparent $CuAlO_2$ delafossite[3,4] has given a boost to the search for new *p*-type TCOs with higher hole conductivity. The main direction for this search has been to explore the family of $CuMO_2$ and $AgMO_2$ delafossite oxides, among which several new *p*-type TCOs have been identified, including $CuGaO_2$,[5] Ca-doped $CuInO_2$,[6] $CuBO_2$,[7] and $CuCrO_2$.[8] Compounds not based on the delafossite structure type have also been studied as candidate *p*-type TCOs. The oxy-chalcogenides have received great attention after the discovery of the transparency and *p*-type conductivity of LaCuOS,[9] which has a layered structure in which CuS layers alternate with LaO layers. $SrCu_2O_2$ has also been proposed and characterized as a candidate *p*-type TCO.[10] Further, $ZnRh_2O_4$[11] and Ni_2CoO_4,[12] which have the spinel structure, have attracted much attention recently. However, so far the search for new *p*-type TCOs has proceeded by chemical insight rather than through the application of a search protocol based on design principles (DPs).

In Ref. 13, we suggested a procedure to search for *p*-type TCOs in which large families of compounds were screened in order to find those that meet the DPs for *p*-type TCOs. We started from the prototype *p*-type binary oxides (Ag_2O and Cu_2O) and defined a large set of ternary materials to screen. We found that the optical and transport properties of Ag_3VO_4 along with a range of conditions in which it can be synthesized better satisfy the DPs than the "parent" Ag_2O binary oxide. However, the intrinsic *p*-type conductivity of Ag_3VO_4 is not high enough, owing to the low equilibrium hole content, and the optical bandgap is not large enough for transparency to visible light. To search for a material with better transport and optical properties compared to those of Ag_3VO_4, one may screen the other compounds in the Ag–V–O space with different composition. The search strategy we follow here is to survey quaternary compounds containing Ag, V, O, and an additional atom in order to identify materials that

a)Electronic mail: j-im@northwestern.edu

 © 2013 AIP Publishing LLC

Downloaded 24 Jun 2013 to 192.174.37.50. This article is copyrighted as indicated in the abstract. Reuse of AIP content is subject to the terms at: http://jcp.aip.org/about/rights_and_permissions

comply with the DPs. A survey of these quaternary oxides led us to identify $KAg_{11}(VO_4)_4$,[14] with a crystal structure related to that of Ag_3VO_4. In $KAg_{11}(VO_4)_4$, all the O atoms form strong bonds with the 4-fold coordinated V atoms that, as in Ag_3VO_4, should make the formation of intrinsic O vacancies energetically unfavorable. At the same time, the 2- and 3-fold coordinated Ag atoms in $KAg_{11}(VO_4)_4$ should exhibit a lower defect formation energy than the 4-fold ones and this should facilitate the formation of the hole-producing Ag vacancies at these lower coordination sites. These local bonding features make $KAg_{11}(VO_4)_4$ an interesting case study of a quaternary oxide as a candidate *p*-type TCO.

In this work, we used first-principles calculations to investigate the thermodynamic stability and the band-structure-related properties of bulk $KAg_{11}(VO_4)_4$, as well as the formation energy and concentration of the main intrinsic hole producing and hole killing defects. Also, we carried out synthesis and experimental characterization of $KAg_{11}(VO_4)_4$. We then compare $KAg_{11}(VO_4)_4$ with Ag_3VO_4 and discuss how the presence of the additional element, K, and the various bonding geometries at the Ag sites in $KAg_{11}(VO_4)_4$ affect both the defect chemistry and its ability to meet the DPs for *p*-type TCOs.

II. METHODS

In order to investigate the electronic structure, optical properties, and defect energetics, we carried out first-principles electronic structure calculations within the density functional theory (DFT) formalism. We used the plane-wave basis set and pseudo-potential scheme with the projector augmented wave method[15,16] as implemented in the *Vienna ab initio Simulation Package* (VASP) code.[17,18] The plane wave cut-off energy was set to 550 eV for the electronic structure and defect formation energy calculations. For the optimization of the internal coordinates and lattice parameters, the cut-off energy was set to 700 eV. A larger energy cutoff decreases the possible error on the stress tensor components which results from the changing volume during the optimization of the lattice vectors. We used the generalized gradient approximation (GGA) with the Perdew-Burke-Ernzerhof formalism[19] for the exchange correlation functional with an on-site Coulomb interaction between the *d*-orbitals of the transition metal atoms. The value of the Coulomb-interaction parameter U was set equal to 6.2 eV for Ag and to 2.2 eV for V. These U values were chosen so as to reproduce the correct ordering of the heat of formation of the Ag and V binary oxide phase.[13,20] For the Brillouin zone sampling, a regular **k**-point mesh was chosen by the Monkhorst-Pack scheme[21] with a density of 25 for the relaxation of the crystal structure, of 50 for calculating total energy and the density of states, and of 100 per unit length of the reciprocal space for the calculating optical and transport properties. The optical absorption coefficient $\alpha(\omega)$ was obtained from the frequency-dependent dielectric function $\varepsilon(\omega)$ which was calculated by using the longitudinal pseudo-potential approach.[22]

The formation energy $\Delta H_{D,q}$ of a point defect D with charge q in thermodynamic equilibrium was calculated by the formula

$$\Delta H_{D,q} = \left[(E_{D,q} - E_H) + qE_V + \sum n_\alpha \mu_\alpha^0\right] + \left[q\Delta E_F + \sum n_\alpha \Delta\mu_\alpha\right], \quad (1)$$

where $E_{D,q}$ and E_H are the total energies of the system including defect (D) with charge q and the pristine host system, respectively; E_V is the energy of the valence band maximum (VBM); n_α is the number of atoms of element α being removed from the supercell to the reservoir; μ_α^0 is the total energy of α in the elemental solid or gas phase; ΔE_F is the Fermi level (the electron chemical potential) referenced to E_V; $\Delta\mu_\alpha$ is the chemical potential of α relative to μ_α^0. The first term in Eq. (1) defines a "defect formation energy which is independent of thermodynamic variables" ($\Delta H_{D,q}^0$), and the remaining terms indicate the dependence of the defect formation energy on the Fermi level and the chemical potentials of the reservoirs of elements, respectively, due to finite temperature and the thermodynamic equilibrium condition with other competing phases. The total energy of a defect system was calculated by using finite supercells. In order to correct the error from the finite cell size, we added correction terms: the band-filling effect and the image charge correction. The band-filling effect originates from the finite cell size, and the image charge correction comes from the interaction of charged defects. Technical details of these corrections can be found in Refs. 23 and 24. The charge transition level $\varepsilon(q/q')$ between charge states q and q' of defect D corresponds to the electron chemical potential E_F for which the formation energy for the charge states q and q' of the defect D are equal, i.e., $\Delta H_D(E_F; q) = \Delta H_D(E_F; q')$. According to Eq. (1), the charge transition level was calculated by $\varepsilon(q/q') = [\Delta H_D(E_V; q') - \Delta H_D(E_V; q)]/(q - q')$. The equilibrium concentration of a defect D with charge state q was determined by $\rho_{D,q} = N_{site} exp(-\Delta H_D(E_F, q)/k_B T)$, where N_{site} is the number of defect sites per unit volume. Finally, E_F was self-consistently determined by the charge neutrality condition at a given temperature, T, which requires that the total charge from the free carriers equal the total charge from the charged defects.

For the experimental measurement on the optical band edge of $KAg_{11}(VO_4)_4$, polycrystalline $KAg_{11}(VO_4)_4$ powders were prepared by a low temperature hydrothermal synthesis. Ag_2O (Fisher Chemical, laboratory grade), V_2O_5 (Alfa Aesar, 99.6% min), and KOH (Sigma-Aldrich, 90%, reagent grade) were mixed in a 1:1:3 (Ag_2O: V_2O_5: KOH) molar ratio and put into a fluoro(ethylene-propylene) (FEP) Teflon pouch. The pouches were heat-sealed before loading them into the autoclave. The function of KOH is twofold: KOH regulates the amount of water that diffuses into the pouch and it also functions as a mineralizer, which facilitates the dissolution of the metal ions at an increased pH. Up to seven pouches were placed in a 125 ml autoclave with a Teflon liner, which was backfilled with 50 ml water. The autoclave was closed and heated at 433 K for 50 h and cooled down to room temperature at 0.1 K/min to maximize growth. After the synthesis, the powders were washed three times with distilled water to remove all traces of KOH. A diffuse reflectance

Downloaded 24 Jun 2013 to 192.174.37.50. This article is copyrighted as indicated in the abstract. Reuse of AIP content is subject to the terms at: http://jcp.aip.org/about/rights_and_permissions

spectrometer was used to obtain data on optical properties such as the bandgap. A Perkin-Elmer Lambda1050 instrument with an integrated sphere was used to collect diffuse reflectance data over the spectral range of 250–800 nm with a data interval of 1 nm. A baseline was collected using a slit width of 2 mm at 650 nm. By fitting a line to the high-energy edge of the top of the diffuse reflectance and taking the intersection of this line with the fitted curve to the low-energy end of the spectrum, the value of the bandgap is obtained.

III. SPACE OF CANDIDATE QUATERNARY COMPOUNDS AND SELECTION OF $KAg_{11}(VO_4)_4$

As an extended space of the ternary compounds defined in Ref. 13, we established the set of quaternary materials following the relation:

$$n\mathrm{Ag_2O} + m\mathrm{V_2O_5} + l M_2\mathrm{O}_\lambda \rightarrow \mathrm{Ag}_{2n}\mathrm{V}_{2m}M_{2l}\mathrm{O}_{n+5m+l\lambda}, \quad (2)$$

where M is a third *cation* species (different from Ag or V) with oxidation number l. In relation (2), the species of the M element, its valence state λ, and the indices, n, m, and l, are the degrees of freedom that formally define quaternary silver vanadium oxides. By surveying the Inorganic Crystal Structure Database[25,26] (ICSD), we found 23 known quaternary oxides following the relation (2). Among these 23 materials, $KAg_{11}(VO_4)_4$ is the one with a crystal structure that can be thought of as derived from the crystal structure of Ag_3VO_4. For the present study, we selected $KAg_{11}(VO_4)_4$ as a case study of the application of the DPs for optimal p-type TCOs among the class of quaternary materials, because of several structural features explained in next paragraph.

$KAg_{11}(VO_4)_4$ has an orthorhombic crystal structure with the space group D_{2h}^{15} (*Pbca*) and 4 formula units in the unit cell.[14] To explain features of the crystal structure of $KAg_{11}(VO_4)_4$, we compare it to that of the α-phase of Ag_3VO_4 (α-Ag_3VO_4). As shown in the left panels of Figs. 1(a) and 1(b), the cation atoms are ordered on the fcc-sublattice (depicted as thick blue lines) both in $KAg_{11}(VO_4)_4$ and α-Ag_3VO_4. However, the local geometries around the Ag atoms are different. In $KAg_{11}(VO_4)_4$, there exist 2-fold, 3-fold, and 4-fold coordinated Ag-sites (Fig. 1(a)), while there are only 4-fold coordinated Ag-sites in Ag_3VO_4 (Fig. 1(b)). Since Ag-vacancies (V_{Ag}) are predicted to be the major source of holes in α-Ag_3VO_4,[13] one may think that a different local geometry of the Ag vacancies affects the concentration of such defects in the material, and thus it may lead to a modification of the p-type transport properties. In this respect, $KAg_{11}(VO_4)_4$ is a system that allows us to verify how the different coordination of the transition metals with respect to Ag_3VO_4 affects the hole content and thermodynamic stability, both properties are needed to be optimized in p-type TCOs.

IV. RESULTS

A. Thermodynamic stability of $KAg_{11}(VO_4)_4$

For a compound to form at a given temperature and pressure, it must be thermodynamically more stable than any of the other compounds, the so-called "competing" phases

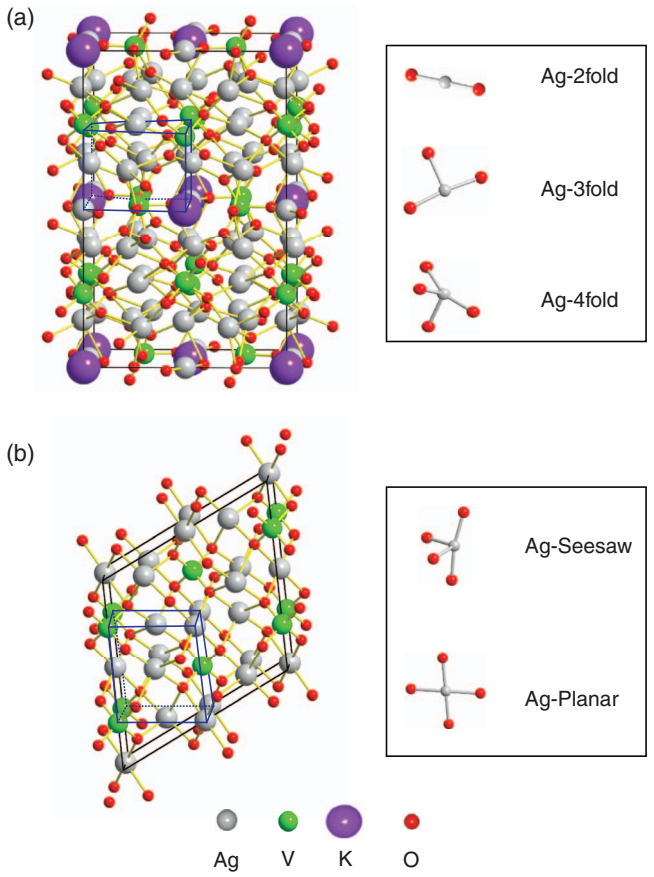

FIG. 1. Atomic structures of (a) $KAg_{11}(VO_4)_4$ (left hand side) and three different local structures of Ag (right hand side), and (b) atomic structures of Ag_3VO_4 (left hand side) and local structures of Ag atom (right hand side). Silver-, green-, purple-, and red-colored spheres denote Ag, V, K, and O atom, respectively. Thick blue lines represent fcc-ordered cations.

which are composed of the same set of elements. The competing phases of $KAg_{11}(VO_4)_4$ include the pure phases of K, Ag, V, and O, the binary oxides of Ag, K, and V, and the ternary oxides of Ag–V–O, K–V–O, and Ag–K–O systems. The conditions for thermodynamic stability of $KAg_{11}(VO_4)_4$ are, thus, expressed by the following relations:

$$\Delta\mu_\mathrm{K} + 11\Delta\mu_\mathrm{Ag} + 4\Delta\mu_\mathrm{V} + 16\Delta\mu_\mathrm{O} = \Delta H_f(\mathrm{KAg_{11}(VO_4)_4}), \quad (3a)$$

$$\Delta\mu_\mathrm{K} \le 0, \quad \Delta\mu_\mathrm{Ag} \le 0, \quad \Delta\mu_\mathrm{V} \le 0, \quad \Delta\mu_\mathrm{O} \le 0, \quad (3b)$$

$$n\Delta\mu_A + m\Delta\mu_\mathrm{O} \le \Delta H_f(A_n\mathrm{O}_m), \quad (3c)$$

$$n'\Delta\mu_A + m'\Delta\mu_B + l'\Delta\mu_\mathrm{O} \le \Delta H_f(A_{n'}B_{m'}\mathrm{O}_{l'}), \quad (3d)$$

where A, B = K, Ag, and V. $\Delta\mu_\alpha$ is the difference between the chemical potential μ_α of element α and the chemical potential μ_α^0 of the most stable phase of α. ΔH_f indicates the heat of formation of a compound considered in the relations (3), defined as $\Delta H_f = E_{tot} - \sum_\alpha n_\alpha \mu_\alpha^0$, where E_{tot} is the total energy of the compound. Equation (3a) represents the condition of thermodynamic equilibrium of the *target* phase, $KAg_{11}(VO_4)_4$. The inequalities (3b)

Downloaded 24 Jun 2013 to 192.174.37.50. This article is copyrighted as indicated in the abstract. Reuse of AIP content is subject to the terms at: http://jcp.aip.org/about/rights_and_permissions

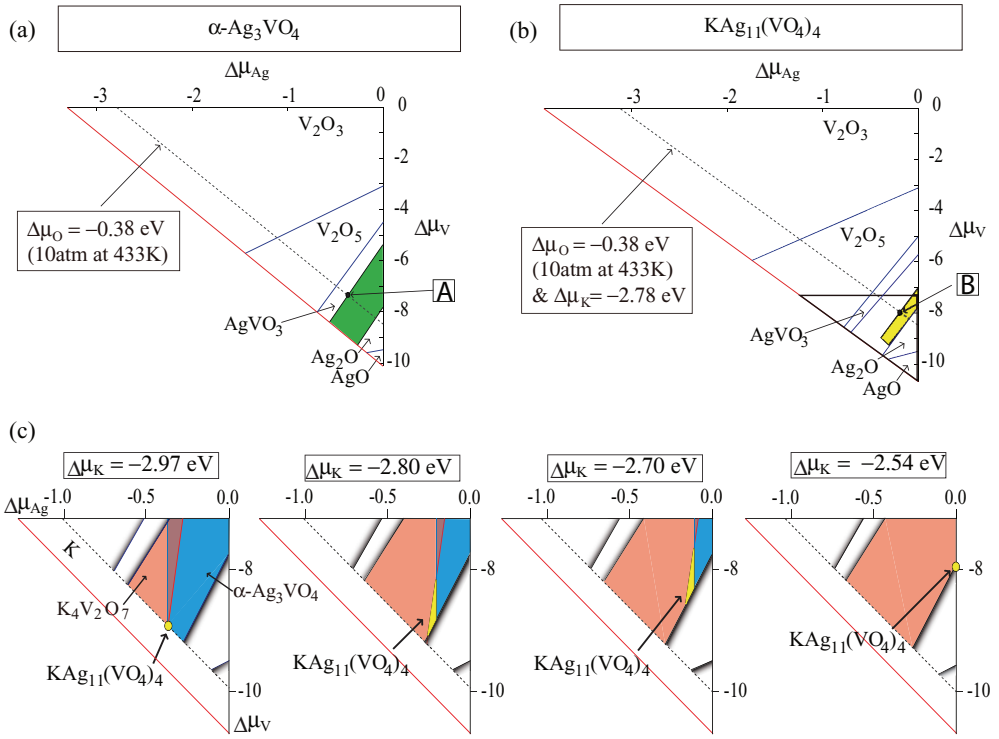

FIG. 2. Calculated thermodynamic stability plot for (a) Ag_3VO_4, (b) $KAg_{11}(VO_4)_4$, and (c) additional competing materials in $KAg_{11}(VO_4)_4$ as a function of $\Delta\mu_K$. In (a) and (b), the chemical potential of Ag is on the x axis and the chemical potential of V is on the y axis. The blue lines denote the boundaries between competing compounds (V_2O_3, V_2O_5, $AgVO_3$, Ag_2O, and AgO) and target compounds (Ag_3VO_4 and $KAg_{11}(VO_4)_4$). The stable region of the target compound is represented by the green region for Ag_3VO_4 in (a) and the yellow area for $KAg_{11}(VO_4)_4$ in (b). The dotted lines denote the growth condition where $\Delta\mu_O = -0.38$ eV in (a) and $\Delta\mu_O = -0.38$ eV and $\Delta\mu_K = -2.78$ eV in (b). The "Ag-poor" conditions are shown as black points in (a) and (b), which are denoted by A and B, respectively. The black-lined triangle around the yellow region in (b) is explained in detail in (c). In (c), the boundaries between the pure K phase and $KAg_{11}(VO_4)_4$ are denoted by dotted lines. The regions restricted by $K_4V_2O_7$, and α-Ag_3VO_4 are depicted as red, and blue areas, respectively. The plots are depicted for $\Delta\mu_K = -2.97$ eV, $\Delta\mu_K = -2.80$ eV, $\Delta\mu_K = -2.70$ eV, and $\Delta\mu_K = -2.54$ eV. The stable areas of $KAg_{11}(VO_4)_4$ are denoted by yellow.

are the conditions for the pure phases of the elemental constituents to be energetically unfavorable. The inequalities (3c) and (3d) express the conditions that all possible competing binary and ternary compounds must be unstable with respect to the formation of $KAg_{11}(VO_4)_4$. Equation (3a) and the inequalities (3b)–(3d) define a constrained linear system whose solutions are the chemical potential of the elements for which $KAg_{11}(VO_4)_4$ is thermodynamically stable.

The region of allowed chemical potentials obtained by solving the linear equation and inequalities (3a)–(3d) is shown in Figs. 2(a) and 2(b) for α-Ag_3VO_4 and $KAg_{11}(VO_4)_4$, respectively, by the green and yellow areas. In order to facilitate the visualization of the region of stability of $KAg_{11}(VO_4)_4$, we project it along the $\Delta\mu_K$ axis. In Fig. 2(a), the intervals of $\Delta\mu_\alpha$ for the thermodynamic stability of α-Ag_3VO_4 are restricted by competing phases, V_2O_3, V_2O_5, Ag_2O, AgO, and $AgVO_3$. In Fig. 2(b), however, the intervals of $\Delta\mu_\alpha$ for the thermodynamic stability of $KAg_{11}(VO_4)_4$ are restricted by additional competing phases including elemental K and other ternary compounds. Since the boundaries between $KAg_{11}(VO_4)_4$ and these competing phases change noticeably as a function of $\Delta\mu_K$, we plotted separately those boundaries for a few values of $\Delta\mu_K$ in Fig. 2(c). We observe that the region of stability of $KAg_{11}(VO_4)_4$ is bound by K, $K_4V_2O_7$, α-Ag_3VO_4, and Ag_2O. This result indicates that additional K-based silver oxide competing phases restrict the stability of $KAg_{11}(VO_4)_4$ within a narrower range of $\Delta\mu_{Ag}$ (−0.37 eV to 0.00 eV) compared to that of α-Ag_3VO_4 (−0.50 eV to 0.00 eV), and thus the conditions of synthesis of $KAg_{11}(VO_4)_4$ are further limited.

In the experimental synthesis of α-Ag_3VO_4 and $KAg_{11}(VO_4)_4$, we used the same growth conditions of T (= 433 K) and pO_2 (= 10 atm). Under these conditions, the corresponding $\Delta\mu_O$ is −0.38 eV (see Ref. 27). The condition of $\Delta\mu_O = -0.38$ eV is displayed as a dotted line in Figs. 2(a) and 2(b). Once $\Delta\mu_O$ is determined, in order to maximize the concentration of metal vacancies, we considered the "metal-poor" condition corresponding to minimum values of the chemical potential of the metal. Then, point A (in Fig. 2(a)) and point B (in Fig. 2(b)) are established from the adjoining points of the dotted line and the stable region of α-Ag_3VO_4 and $KAg_{11}(VO_4)_4$, respectively. The corresponding chemical potentials of Ag are $\Delta\mu_{Ag} = -0.19$ eV for $KAg_{11}(VO_4)_4$ and $\Delta\mu_{Ag} = -0.31$ eV for Ag_3VO_4. In Sec. IV B, we evaluate the defect formation energy relative to the condition defined by the chemical potentials of points A and B in Figs. 2(a) and 2(b), respectively.

B. Defect-formation energy and hole-concentration

There are several point defects that can contribute to the intrinsic hole content in α-Ag_3VO_4 and $KAg_{11}(VO_4)_4$.

Downloaded 24 Jun 2013 to 192.174.37.50. This article is copyrighted as indicated in the abstract. Reuse of AIP content is subject to the terms at: http://jcp.aip.org/about/rights_and_permissions

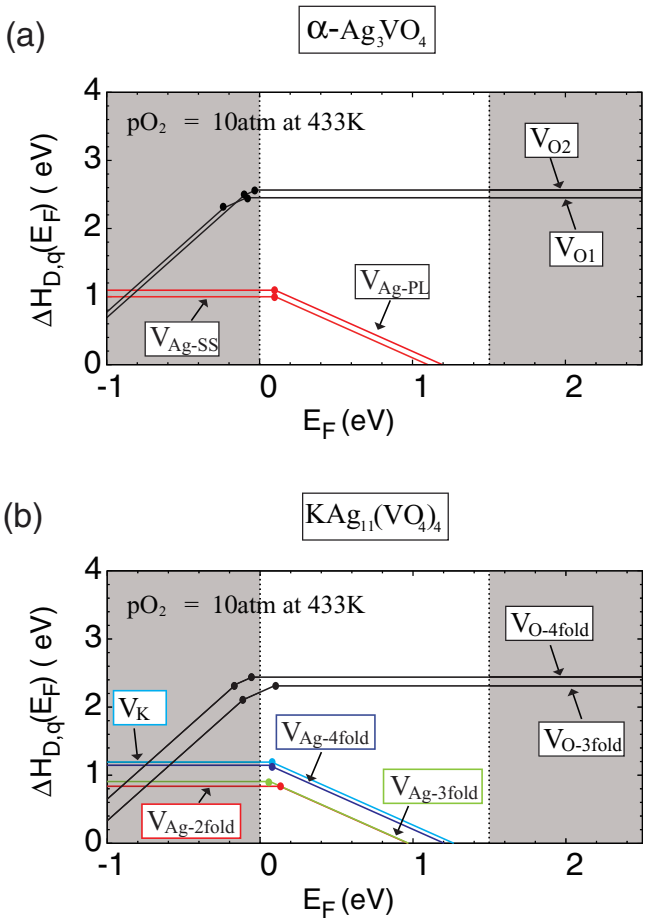

FIG. 3. Calculated defect-formation energies in (a) Ag_3VO_4 and (b) $KAg_{11}(VO_4)_4$. The x axis stands for the Fermi energy and the zero energy is set to the VBM. The y axis stands for the defect-formation energy. In (a), the two black lines denote the defect formation energies of O vacancies and the two red lines represent the formation energies of the Ag vacancies. In (b), the two black lines denote the formation energies of O-vacancies and the red, green, dark blue, and light blue lines represent the defect formation energy of 2-fold Ag vacancy, 3-fold Ag vacancy, 4-fold Ag vacancy, and K vacancy, respectively. The gray-colored region represents the valence band (left hand side) and conduction band (right hand side).

We considered single cation vacancies of Ag^+, V^{5+}, K^+. The oxygen vacancies are donor defects, that compensate the hole produced by the metal vacancies. We take the experimental growth conditions (pO_2 = 10 atm and T = 433 K) and set $\Delta\mu_{Ag}$ and $\Delta\mu_K$ to Ag-poor and K-poor conditions. These conditions are represented by the points A for α-Ag_3VO_4 and B for $KAg_{11}(VO_4)_4$ on the thermodynamic stability plots, Figs. 2(a) and 2(b), respectively. Figures 3(a) and 3(b) show the calculated formation energies of vacancy defects as a function of the electron chemical potential ΔE_F. In α-Ag_3VO_4, we considered two kinds of Ag vacancies (V_{Ag}) on a planar-like (PL) site and a seesaw-like (SS) site, and two kinds of O-vacancies (V_O) on the two different Wykoff positions of oxygen. The V_{Ag} serves as a source of holes, while V_O acts as a hole-killing defect. The vanadium vacancy (V_V) in the neutral charge state has a formation energy higher than 4 eV and, thus, is unlikely to form. The formation energies of the two Ag-vacancies V_{Ag} in α-Ag_3VO_4 are relatively low compared to those of neutral V_O and the transition level $\varepsilon(0/-)$ of V_{Ag} is just above the VBM. On the other hand, the transition level $\varepsilon(+/0)$ of V_O are below the VBM; thus for any ΔE_F in the gap, the V_O have high formation energies, which make them difficult to form and are neutral (do not release electrons) in correspondence with the ΔE_F at which the hole producing defects become electrically charged by releasing holes. The high formation energy of V_O is due to the strong bond between vanadium and oxygen atoms in the tetrahedral VO_4 units in α-Ag_3VO_4.[13]

In the case of $KAg_{11}(VO_4)_4$, we investigated the defect physics of V_{Ag} at the 2-, 3-, and 4-fold coordinated Ag sites, V_O of the 3-/4-fold O site, V_K, and V_V. As shown in Fig. 3(b), the hole-producing defects V_{Ag} and V_K in $KAg_{11}(VO_4)_4$ have relatively low defect formation energies as compared to the V_O and have shallow acceptor levels similar to the V_{Ag} in α-Ag_3VO_4. In addition, the defect formation energies of the 2-fold and 3-fold coordinated V_{Ag} defects are smaller than the formation energy of the 4-fold coordinated V_{Ag} in $KAg_{11}(VO_4)_4$. This difference is likely related to the number of bonds broken in each case in order to form a V_{Ag}; this leads to a higher concentration of the 2-/3-fold coordinated V_{Ag} than the 4-fold coordinated one in $KAg_{11}(VO_4)_4$. Thus, the holes in $KAg_{11}(VO_4)_4$ mostly originate from the 2-/3-fold coordinated V_{Ag}. The hole-killing defect V_O in $KAg_{11}(VO_4)_4$ is neutral (does not release electrons) for most values of ΔE_F in the gap and has a rather high defect formation energy; even though the transition level $\varepsilon(+/0)$ of 3-fold V_O is just above VBM, it becomes inactive above ΔE_F = 0.1 eV. Like α-Ag_3VO_4, all oxygen atoms in $KAg_{11}(VO_4)_4$ are strongly bonded to vanadium atoms in the VO_4 tetrahedral structure and this results in the high formation energy of V_O in $KAg_{11}(VO_4)_4$.

The $\Delta H^0_{D,q}$ of the 4-fold coordinated V_{Ag} in $KAg_{11}(VO_4)_4$ is similar to that of V_{Ag} in α-Ag_3VO_4, while the $\Delta H^0_{D,q}$ of the 2- and 3-fold coordinated V_{Ag} is smaller than that of the 4-fold coordinated V_{Ag} both in $KAg_{11}(VO_4)_4$ and α-Ag_3VO_4 (see Table I). However, a smaller $\Delta H^0_{D,q}$ of the 2-/3-fold coordinated V_{Ag} in $KAg_{11}(VO_4)_4$ does not translate into a higher concentration of V_{Ag} and of holes in $KAg_{11}(VO_4)_4$. Indeed, once the formation energies are calculated via Eq. (1), taking into account the chemical potential of Ag in the thermodynamic equilibrium state corresponding to the targeted experimental growth conditions, then the values of $\Delta H_{D,q}$ of the 2-/3-fold coordinated V_{Ag} in $KAg_{11}(VO_4)_4$ become comparable with that of V_{Ag} in α-Ag_3VO_4. In Fig. 4, we plot the calculated hole concentration of $KAg_{11}(VO_4)_4$ and α-Ag_3VO_4 as a

TABLE I. Calculated defect formation energy which is independent of thermodynamic variables ($\Delta H^0_{D,q}$) for Ag vacancies of Ag_3VO_4 and $KAg_{11}(VO_4)_4$.

	Vacancy	$\Delta H^0_{D,q}$ (eV)
Ag_3VO_4	4-fold Ag (PL)	1.41
	4-fold Ag (SS)	1.31
$KAg_{11}(VO_4)_4$	2-fold Ag	1.02
	3-fold Ag	1.09
	4-fold Ag	1.33

Downloaded 24 Jun 2013 to 192.174.37.50. This article is copyrighted as indicated in the abstract. Reuse of AIP content is subject to the terms at: http://jcp.aip.org/about/rights_and_permissions

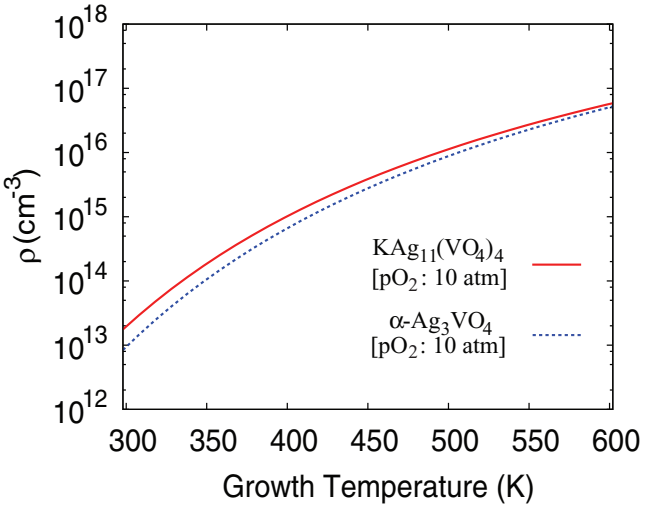

FIG. 4. Calculated hole concentration in α-Ag_3VO_4 and $KAg_{11}(VO_4)_4$. The x axis denotes the growth temperature and the y axis the carrier concentration; the red line indicates the hole concentration in $KAg_{11}(VO_4)_4$ and the dashed blue line that of α-Ag_3VO_4.

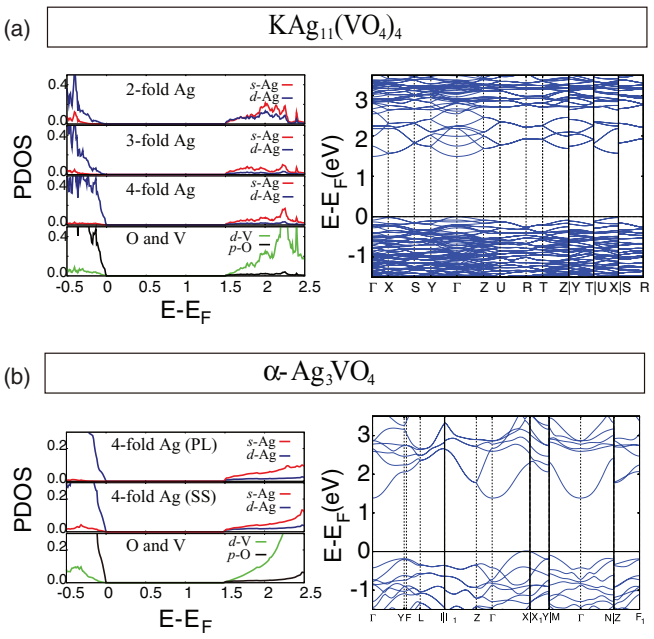

FIG. 5. Calculated electronic band structures and the projected density of states (PDOS) of (a) $KAg_{11}(VO_4)_4$ and (b) Ag_3VO_4. In the left hand side of (a), the density of states of $KAg_{11}(VO_4)_4$ projected onto the 2-fold Ag atom, 3-fold Ag atom, 4-fold Ag atom, O atom, and V atom. In the left hand side of (b), the density of state of Ag_3VO_4 is projected onto the planar (PL) Ag atom, seesaw (SS) Ag atom, O atom, and V atom. In all PDOS plots, red, blue, green, and black lines represent components of the *s*-orbital of Ag, the *d*-orbital of Ag, the *d*-orbital of V, and the *p*-orbital of O, respectively.

function of temperature at the experimental oxygen partial pressure ($pO_2 = 10$ atm). At room temperature, the combined contribution of the 2-, 3-, and 4-fold coordinated V_{Ag} defects results in a hole concentration of 1.76×10^{13} cm^{-3} in $KAg_{11}(VO_4)_4$ and 0.84×10^{13} cm^{-3} in α-Ag_3VO_4. The hole concentration is larger in $KAg_{11}(VO_4)_4$ than in α-Ag_3VO_4 by a factor of 2, but this is a gain that does not satisfy the desired hole concentrations for a *p*-type TCO (i.e., 10^{18} cm^{-3}).

C. Hole effective mass and optical properties

We now proceed to assess the transport and optical properties of $KAg_{11}(VO_4)_4$ and contrast them with those of α-Ag_3VO_4. Figure 5 compares the band structures and the projected density of states (PDOS) of $KAg_{11}(VO_4)_4$ and α-Ag_3VO_4. $KAg_{11}(VO_4)_4$ has a direct bandgap of 1.50 eV at Γ, while α-Ag_3VO_4 has an indirect bandgap of 1.34 eV. From the PDOS on the left hand side of Figs. 5(a) and 5(b), we note that in both $KAg_{11}(VO_4)_4$ and α-Ag_3VO_4 the electronic states near the VBM mainly derive from Ag-*d* orbitals located at the 4-fold coordinated Ag-site and from O-*p* orbitals; the 2-fold and 3-fold coordinated Ag-sites in $KAg_{11}(VO_4)_4$ do not contribute noticeably to the VBM. On the other hand, in both compounds, the conduction band minimum (CBM) consists of the Ag-*s* orbital and the V-*d* orbital as shown in Figs. 5(a) and 5(b). Therefore, both $KAg_{11}(VO_4)_4$ and α-Ag_3VO_4 have similar orbital compositions at the VBM and CBM.

As a result, physical properties coming from band edges, such as mobility and the optical absorption edge, could be comparable in both compounds. In regard to the hole mobility, we evaluate the "density of states" effective mass m^*_{DOS} (see details in Ref. 13). This quantity is useful to explain features of the band extrema when the band dispersion is anisotropic and non-parabolic, as in α-Ag_3VO_4 and $KAg_{11}(VO_4)_4$. When we assume T = 300 K, the m^*_{DOS} at the VBM is 2.91 m_e for $KAg_{11}(VO_4)_4$ and 2.54 m_e for α-Ag_3VO_4, so they are comparable to each other. In Fig. 6, we compare the optical absorption spectra $\alpha(\omega)$ of $KAg_{11}(VO_4)_4$ and α-Ag_3VO_4. The calculated absorption edge of $KAg_{11}(VO_4)_4$ is 1.5 eV (Fig. 6(a)) and from the band structure in Fig. 5(a) we observe that the optical gap of $KAg_{11}(VO_4)_4$ originates from the direct transition between the VBM and CBM at Γ. In the case of α-Ag_3VO_4, the absorption edge is 1.7 eV (Fig. 6(b)) and it corresponds to a direct transition near Γ (Fig. 5(b)).

Because our calculation method usually underestimates the value of the optical bandgap (as is typical of local density approximation (LDA) and GGA), in order to determine the optical properties more exactly, we performed diffuse reflectance spectroscopy measurements on a pressed pellet of $KAg_{11}(VO_4)_4$. The optical bandgap of the $KAg_{11}(VO_4)_4$ pellet can be determined by plotting the Kubelka-Munk function as a function of energy (Fig. 6(c)). The obtained optical bandgap is 2.0 eV for $KAg_{11}(VO_4)_4$ and 2.1 eV for Ag_3VO_4. This result shows that the trend in experimental results is consistent with that of the calculated optical gaps.

V. DISCUSSION AND CONCLUSION

In this paper, a theory-based search, driven by DPs, to identify a new candidate *p*-type TCO was performed. The search strategy consisted of surveying a nontrivial materials space to identify materials that meet the DPs. First, we established a set of requirements which should be satisfied by optimal *p*-type TCOs; we then expanded the materials space to screen quaternary oxides defined by using relation (2). In doing so, we surveyed the set of known quaternary compounds including Ag, V, and O, from which $KAg_{11}(VO_4)_4$ emerged

Downloaded 24 Jun 2013 to 192.174.37.50. This article is copyrighted as indicated in the abstract. Reuse of AIP content is subject to the terms at: http://jcp.aip.org/about/rights_and_permissions

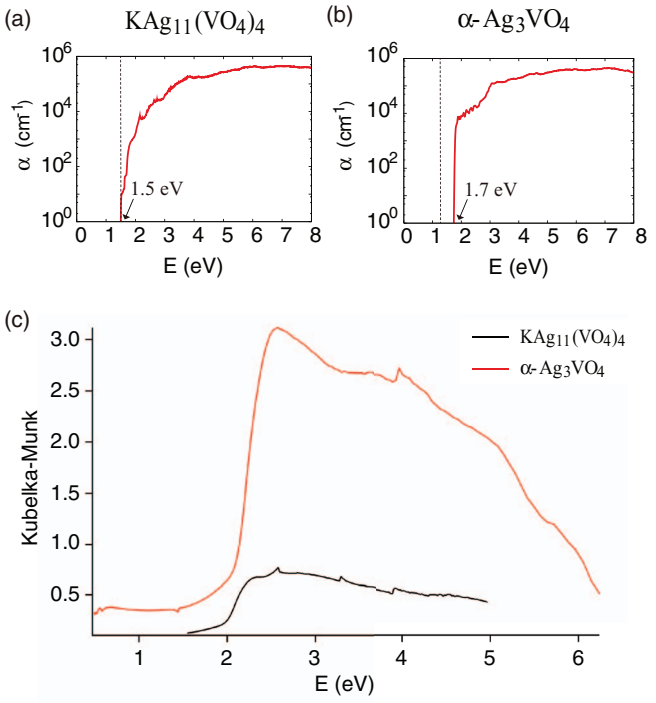

FIG. 6. Calculated optical absorption coefficients of (a) $KAg_{11}(VO_4)_4$ and (b) Ag_3VO_4, and (c) experimental diffuse reflectance spectra of $KAg_{11}(VO_4)_4$ and Ag_3VO_4. In (a) and (b), dotted lines indicate fundamental gaps from band structures.

as a material with composition close to that of α-Ag_3VO_4, but with different local geometries of the Ag sites, which might result in different, possibly improved, properties over those of Ag_3VO_4.

Our calculation showed that $KAg_{11}(VO_4)_4$ is an intrinsic *p*-type compound. The main intrinsic sources of holes are vacancies of 2-fold and 3-fold coordinated Ag atoms. However, the formation energy of the defects in $KAg_{11}(VO_4)_4$ is not low enough to create a large hole concentration, which is 1.76×10^{13} cm^{-3} at 300 K. For the optical absorption edge, our experimental results confirmed the insufficient optical bandgap of $KAg_{11}(VO_4)_4$ for a *p*-type TCO. The optical bandgap of $KAg_{11}(VO_4)_4$ is observed to be 2.0 eV which is reddish and barely transparent.

We also assessed how the different local geometries around the Ag atoms affect the transport properties in Ag_3VO_4 and $KAg_{11}(VO_4)_4$. One may expect that the formation energy of a 2-fold/3-fold coordinated V_{Ag} is lower than that of a 4-fold coordinated V_{Ag} in α-Ag_3VO_4 because the 2-fold and 3-fold coordination of the Ag atoms in $KAg_{11}(VO_4)_4$ leads to a decreased of $\Delta H^0_{D,q}$ of the Ag vacancies. However, the additional competing phases containing the K atoms prevent such vacancies from being formed with low enough formation energy at the thermodynamic equilibrium. Accordingly, at the actual experimental growth condition, $\Delta H_{D,q}$ of 2-fold/3-fold coordinated V_{Ag} in $KAg_{11}(VO_4)_4$ are close to, but slightly lower than those of 4-fold coordinated V_{Ag} in α-Ag_3VO_4, and, as a result, the hole concentration of $KAg_{11}(VO_4)_4$ is increased by only $\sim 10^{13}$ cm^{-3} at room temperature compared to that of α-Ag_3VO_4. Therefore, the lower coordination number on Ag sites in $KAg_{11}(VO_4)_4$ with respect to α-Ag_3VO_4 is overall not beneficial for enhancing the concentration of Ag-vacancies.

ACKNOWLEDGMENTS

This work was supported by the U.S. Department of Energy, Office of Science, Office of Basic Energy Sciences under Contract No. DE-AC36-08GO28308 to NREL. The Center of Inverse Design is a DOE Energy Frontier Research Center.

[1] J. F. Wager, D. A. Keszler, and R. E. Presley, *Transparent Electronics* (Springer, New York, 2008).
[2] *Handbook of Transparent Conductors*, edited by D. S. Ginley, H. Hosono, and D. C. Paine (Springer, New York, 2011).
[3] H. Kawazoe, M. Yasukawa, H. Hyodo, M. Kurita, H. Yanagi, and H. Hosono, Nature (London) **389**, 939 (1997).
[4] H. Kawazoe, H. Yanagi, K. Ueda, and H. Hosono, MRS Bull. **25**, 28 (2000).
[5] K. Ueda, T. Hase, H. Yanagi, H. Kawazoe, H. Hosono, H. Ohta, M. Orita, and M. Hirano, J. Appl. Phys. **89**, 1790 (2001).
[6] H. Yanagi, T. Hase, S. Ibuki, K. Ueda, and H. Hosono, Appl. Phys. Lett. **78**, 1583 (2001).
[7] M. Snure and A. Tiwari, Appl. Phys. Lett. **91**, 092123 (2007).
[8] R. Nagarajan, A. D. Draeseke, A. W. Sleight, and J. Tate, J. Appl. Phys. **89**, 8022 (2001).
[9] K. Ueda, H. Hiramatsu, H. Ohta, M. Hirano, T. Kamiya, and H. Hosono, Phys. Rev. B **69**, 155305 (2004).
[10] A. Kudo, H. Yanagi, H. Hosono, and H. Kawazoe, Appl. Phys. Lett. **73**, 220 (1998).
[11] H. Ohta, K. Nomura, H. Hiramatsu, K. Ueda, T. Kamiya, M. Hirano, and H. Hosono, Solid-State Electron. **47**, 2261 (2003).
[12] G. J. Exarhos, C. F. Windisch, Jr., K. F. Ferris, and R. R. Owings, Appl. Phys. A **89**, 9 (2007).
[13] G. Trimarchi, H. Peng, J. Im, A. J. Freeman, V. Cloet, A. Raw, K. R. Poeppelmeier, K. Biswas, S. Lany, and A. Zunger, Phys. Rev. B **84**, 165116 (2011).
[14] A. Kovalevskiy and M. Jansen, Z. Anorg. Allg. Chem. **632**, 413 (2006).
[15] P. E. Blöchl, Phys. Rev. B **50**, 17953 (1994).
[16] G. Kresse and D. Joubert, Phys. Rev. B **59**, 1758 (1999).
[17] G. Kresse and J. Hafner, Phys. Rev. B **47**, 558 (1993).
[18] G. Kresse and J. Furthmuller, Phys. Rev. B **54**, 11169 (1996).
[19] J. Perdew, K. Burke, and M. Ernzerhof, Phys. Rev. Lett. **77**, 3865 (1996).
[20] S. Lany, J. Osorio-Guillen, and A. Zunger, Phys. Rev. B **75**, 241203(R) (2007).
[21] H. J. Monkhorst and J. D. Pack, Phys. Rev. B **13**, 5188 (1976).
[22] B. Adolph, J. Furthmüller, and F. Bechstedt, Phys. Rev. B **63**, 125108 (2001).
[23] C. Persson, Y.-J. Zhao, S. Lany, and A. Zunger, Phys. Rev. B **72**, 035211 (2005).
[24] S. Lany and A. Zunger, Phys. Rev. B **78**, 235104 (2008).
[25] G. Bergerhoff and I. D. Brown, in *Crystallographic Databases*, edited by F. H. Allen *et al.* (Hrsg.) (International Union of Crystallography, Chester, 1987).
[26] A. Belsky, M. Hellenbrandt, V. L. Karen, and P. Luksch, Acta Cryst. B **58**, 364 (2002).
[27] J. Osorio, S. Lany, S. V. Barabash, and A. Zunger, Phys. Rev. Lett. **96**, 107203 (2006).

Downloaded 24 Jun 2013 to 192.174.37.50. This article is copyrighted as indicated in the abstract. Reuse of AIP content is subject to the terms at: http://jcp.aip.org/about/rights_and_permissions